Research Article Received: 2024-01-02, Accepted: 2024-04-23

A Functional N/S doped-Carbon Electrode from a Carbonized Bagasse Activated with Water Vapor

Fitria Rahmawati[1*], Ainaya Febi Amalia[1], Arikasuci Fitonna Ridassepri[1,2], Jun Nakamura[2], Younki Lee[3]

[1]Research Group of Solid-State Chemistry & Catalysis, Chemistry Department, Sebelas Maret University, Jl. Ir. Sutami 36 A Kentingan, Surakarta, Indonesia 57126
[2]Department of Engineering Science, The University of Electro-Communications (UEC- Tokyo), 1-5-1 Chofugaoka, Chofu, Tokyo 182-8585, Japan
[3]Department of Materials Engineering and Convergence Technology, Gyeongsang National University, Jinju, Gyeongnam 52828, Republic of Korea

Email: fitria@mipa.uns.ac.id

ABSTRACT

This research used solid waste from sugarcane production, named bagasse, as raw material for a functional carbon electrode. The bagasse was carbonized to produce carbon powder and, following activation with water vapor at 700 ^{o}C. The activated carbon was doped with N and S to improve its electrochemical properties by treating it with thiourea precursor and heating it at 850 ^{o}C under nitrogen flow to produce N/S doped-carbon (NSCE). The produced carbon was then characterized to understand the specific diffraction pattern, molecular vibrations, and surface morphology. The result found that the NSCE showed two broad diffraction peaks at 23^{o} and 43^{o}, corresponding to [002] and [100] crystal planes following JCPDS75-1621. FTIR spectra showed some O-H, C-H, C-O, and C=C peaks. Peaks of C=N, C-N, and S-H demonstrate the presence of N/S within the NSCE. Raman analysis revealed that N/S doping caused structure defects within the single C6 layer networks, providing carbon vacancies ($V_C^{\bullet\bullet\bullet\bullet}$) because of C replacement by N ($N_C^{'}$) and S ($S_C^{''}$). Meanwhile, XPS analysis showed N/S introduction to the C network by revealing peaks at 168.26 eV and 169.55 eV, corresponding to $S2p_{3/2}$ and $S2p_{1/2}$, and 171. 95 eV corresponds to C-SO_3-C, indicating the presence of S within the thiol group attached to the carbon. Meanwhile, N1s are revealed at 402.4 eV and 405.5 eV, confirming pyrrolic nitrogen (N-5) and quaternary nitrogen (N-Q). The electrochemical analysis found that the reaction within the prepared-NSCE/$NaClO_4$/Na was reversible, with an onset potential of 0.1 V vs. Na/Na^+, explaining the intercalation and deintercalation of sodium ions. The sodium battery full cell showed an excellent battery performance with an initial charging-discharging capacity of 720 mAh/g and 570 mAh/g, respectively, at 0.2C. Meanwhile, a cycling test showed the average Coulombic Efficiency of 84.4 % and capacity retention of 57 % after 50 cycles.

Keywords: carbon, biomass, bagasse, electrode, sodium ion battery

INTRODUCTION

Batteries are essential device to support the apparent growth of portable electric devices, electric vehicles, and energy storage for new and renewable energy power plants. Until recently,

DOI: 10.33961/jecst.2024.00017

lithium-ion batteries (LIBs) dominated the battery market; however, nowadays there is a substantial concern with the limited lithium abundance, which is only 0.01 % on Earth, and the price increases fast up to $5000/ton[1]. Following the abundance, the supply, the lower price, and the comparable electrochemical performance to LIBs, sodium-ion batteries (SIBs) are becoming a feasible alternative for LIBs [2,3]. Some previous research on sodium batteries used amorphous or hard carbon (HCs) as anode material due to its high electronic conductivity, good thermal stability, environmental safety [4], and low-cost production [5]. Hard carbon also has a sizeable interlayer spacing of 0.36 - 0.40 nm, a tortuous structure, and contains micropores, which are essential for a potential host material in a secondary battery [6]. However, hard carbon as a host electrode still faces deficiencies for sodium batteries because Na^+ has a larger ionic radius (1.02 Å) than Li+ (0.76 Å) [7], which causes hard Na^+ to intercalate into the carbon microstructure. Therefore, some efforts to increase Na^+ intercalation have been developed, such as by doping N, P, O into nanoporous carbon [8], and N, B co-doping carbon nanosheet [9].

Some researchers have successfully prepared HCs from biomass, such as wood [10], banana peels [11], cotton [12], corn stalk [13], cellulose [14,15], rice husk [16], and sunflower seed shells [17]. Bagasse is a solid waste of sugarcane production with high carbon content consisting of 50 % cellulose, 25 % hemicellulose, and 25 % lignin [18]. The world bagasse production reached almost 100.000 metric tons/year, spread over Brazil, India, China, Thailand, and some countries by 3500 metric tons/year average, i.e., USA, Pakistan, Mexico, Russia, France and Germany [19]. Meanwhile, Indonesia has a huge potential bagasse production of 9.9 – 11.2 million tons/ year [20]. It became our background to investigate the carbon active preparation from bagasse[21–23]. Activation with water vapor was preferred to replace chemical activators such as KOH [24], $ZnCl_2$ [25], and H_3PO_4 [26], considering the lower price and safety reasons for the environment.

DOI: 10.33961/jecst.2024.00017

In this research, the activated carbon that has been investigated previously; was further treated by submitting N and S into the C networks. Thiourea (CH_4N_2S) was used as an N/S precursor. This research aims to increase the electrochemical performance of the bagasse-activated carbon and projects the result as a functional electrode material for secondary battery. Some characterizations investigated the diffraction peaks, the functional groups available within, the indication of structure defects because of N/S doping, and the chemical structure elucidation based on the binding energies revealed from the material. The feasibility of the prepared material as a functional electrode was tested by combining the N/S doped-carbon with Na metal anode, and $NaClO_4$ electrolyte in a CR2023 cell.

METHOD

Preparation of N/S doped-Carbon and Its Characterization

Carbon powder was prepared from bagasse, a solid waste of sugarcane production. The bagasse was washed with water, followed by carbonation at 600 ^oC and then activated at 700 ^oC under water vapor flows, as previously mentioned in our previous publication [23]. The activated carbon from bagasse (ACB) was then mashed and filtered at 100 mesh to get a small, homogenous carbon particle. Next, the produced powder was mixed with thiourea for dual N/S doping at a mass ratio 1:1 of carbon to the precursor with ethanol as solvent. 30 mL of ethanol was added to the mixture of carbon and precursor, stirred for 2 h at room temperature, and then heated in the oven at 80 ^oC for 6 h. After heating in the oven, the mixture was dried, resulting in powder sediment at the flask's bottom. Finally, the powder was heated at 850 ^oC under N_2 gas flow for 2 h to produce a black powder. A similar procedure was done with distilled water as a dispersant.

The powder was then characterized to understand its crystallinity and the specific diffraction peaks through X-ray Diffraction (Rigaku Miniflex 600), the functional groups content by FT-IR analysis (Shimadzu IRrestige-21), XPS (JEOL JPS-9200, MgK_α source, 10

DOI: 10.33961/jecst.2024.00017

kV, 10 mA), and impedance analysis at 20 Hz – 200 kHz (LCR meter EUCOL 20 Hz - 5 MHz) was conducted to understand the resistance (Ω) and the electrical conductivity (S/cm). The undoped carbon was also analysed for comparison.

Preparation of The Electrode Film

A 0.7 g of the prepared powder was mixed with 0.1 g acetylene black (AB) and then crushed until homogenously mixed. The mixture was then dried at 60 ^{o}C for 45 min. A 0.1 g of PVDF was dissolved within 4 mL NMP and stirred until completely dissolved. The NSCE-AB mixture was added gradually under a stirring condition for 3 h until it formed a homogenous slurry. The slurry was then cast on aluminium foil and dried under vacuum at 80 ^{o}C for 12 h in a vacuum oven (B-One Vacuum Oven VOV – 50, 220V/1400 W).

Sodium Battery Fabrication and Battery Test

The electrode film was assembled with $NaClO_4$ electrolytes and a Na metal anode in a coin cell CR2032. The $NaClO_4$ solution was fed into the PTFE membrane by dipping the membrane in 1 M $NaClO_4$ solution in propylene carbonate for a night. All the assembly was conducted within the Argon glove box (KF-40 VGB-1). The fabricated sodium battery was then analyzed by cyclic voltammetry (Corrtest Electrochemical Workstation CS150) under a voltage range of -1 to 4 Volt vs. Na/Na^{+} at 1 mVs^{-1} and 3 mVs^{-1} of scan rate. Galvanostatic charge-discharge test was conducted with NEWARE Battery Testing System (5V1A) at 0.5 to 3 V under various current rates of 0.2C, 0.5C, and 1C (1C= 374 mAh/g) at Room Temperature. The cycling performance test was conducted by running a charge-discharge test for 50 cycles. An impedance analysis (EUCOL LCR meter 20 Hz – 5 MHz) was also applied to the prepared-sodium battery before and after the charge-discharge test. Impedance before and after 50 cycles was measured with LCR meter (EUCOL, 20 Hz – 5 MHz frequencies) to understand the changes after cycling.

DOI: 10.33961/jecst.2024.00017

RESULT AND DISCUSSION

XRD analysis of the prepared carbon resulted in patterns, as shown in Figure 1. The patterns of N/S doped-carbon are like the undoped activated carbon, in which a broaden-peak lying at 2θ at 24 ^{o} corresponds to the [002] crystal plane of carbon (JCPDS #41-1487). The broad peak confirms amorphous carbon, and the similar patterns demonstrate that the carbon characteristic still dominates the after-doping material.

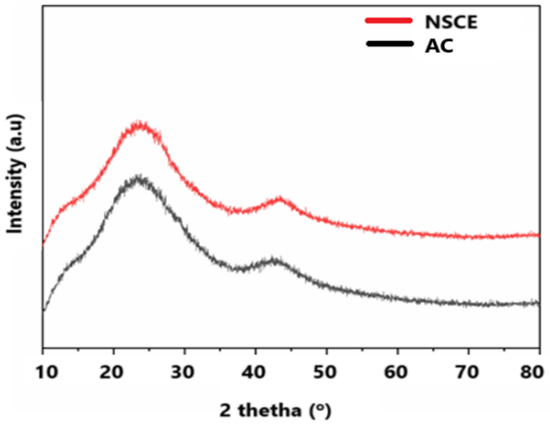

Figure 1. XRD patterns of the doped (NSCE) and undoped carbon (ACB)

Raman analysis of the prepared carbon reveals broad Raman shifting at 1350 cm^{-1} and 1590 cm^{-1}. Raman spectra (Fig. 2) show two broad peaks at 1350 cm^{-1} and 1590 cm^{-1}, confirming the D and G bands [27,28]. The D band reveals that N/S doping caused structure defects within the single C_6 layer networks. Meanwhile, the G band confirms the sp^2 hybridization of C orbitals, representing the carbon material's graphitic degree [29]. The D and G Intensity (I_D/I_G) ratio expresses the degree of carbon defect, in which a high value indicates more defect within the crystal structure. The N/S doping increased the I_D/I_G ratio from 0.92 before doping to 1.15, indicating more defects available after doping. The Kröger-Vink notation in equations (1) theoretically explains the vacancy formation due to the N/S doping.

$$C_6 + N + S \rightarrow 2N_C' + S_C'' + V_C^{\bullet\bullet\bullet\bullet} + 6C_C \qquad (1)$$

DOI: 10.33961/jecst.2024.00017

Equation (1) shows that two N atoms replaced C (N_C), producing two negative charges (′) relative to its initial state, and an atom S replaced C (S_C), creating two negative charges (″) close to its initial state. As a result, carbon vacancies (V_C) formed to bring the network back into neutral charge by compensating with 4 positive charges (••••).

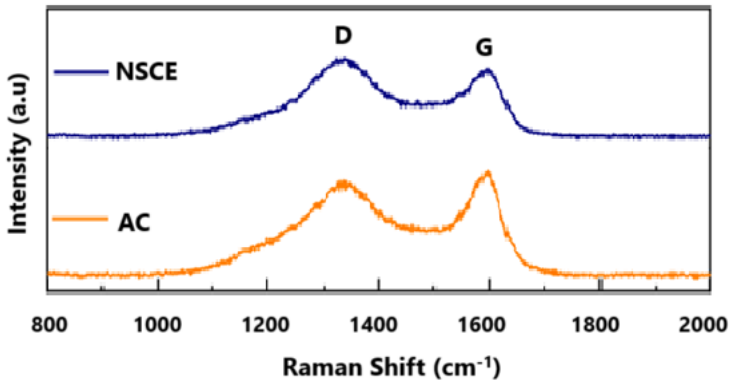

Figure 2. Raman spectrum of the prepared-carbon

EDX mapping (Figure 3) found that NSCE consist of C, O, S, Si, and Cl with composition as listed in Table 1. The result shows that NSCE consist mainly of C with 91.35 atom %, meanwhile S available at 1.61 %. EDX mapping failed to detect light element like nitrogen, N, because of its low photon energy [30]. However, the presence of N in carbon network proven by FTIR analysis as described in Figure 4.

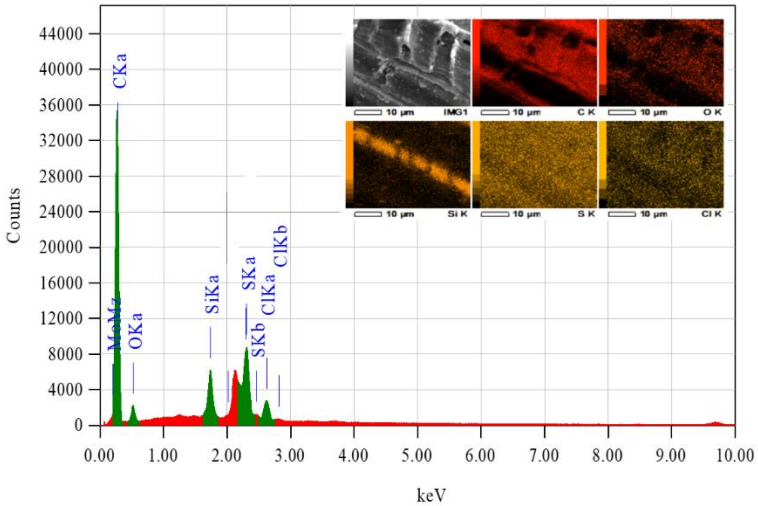

Table 1. Elemental composition of the NSCE

Element	KeV	Mass%	Error %	Atom %
C *K*	0.277	85.36	0.07	91.35
O *K*	0.525	6.73	0.33	5.41
Si *K*	1.739	2.27	0.07	1.04
S *K*	2.307	4.02	0.07	1.61
Cl *K*	2.621	1.63	0.09	0.59

Figure 3. EDX mapping of the prepared-NSCE and its elemental composition (Table 1)

DOI: 10.33961/jecst.2024.00017

FTIR analysis confirms some specific vibrations of carbon, as shown in Fig. 4. The FT-IR spectrum of undoped-carbon or activated-carbon shows characteristic peaks at 3446 cm^{-1} refers to O-H stretching [31,32], C-H stretching at 2884 cm^{-1} [33,34], C-O stretching at 1092 cm^{-1} [32,35], and C=C aromatic at 1570 cm^{-1} [32,34]. The C=C vibrations shift to about 1587 cm^{-1} after N and N/S doping, almost piled up with C=N stretching at around 1534 cm^{-1} [36,37]. The C-N vibration was revealed at about 1048 cm^{-1} and 1066 cm^{-1} [38], and the C-N vibration piled up with C-S at around 1084 cm^{-1} after N/S doping [38]. A broad peak at 3446 cm^{-1} refers to O-H stretching, representing H_2O adsorption onto carbonaceous material, and an O-H group attached to the carbon network around 3418 cm^{-1} [31,32].

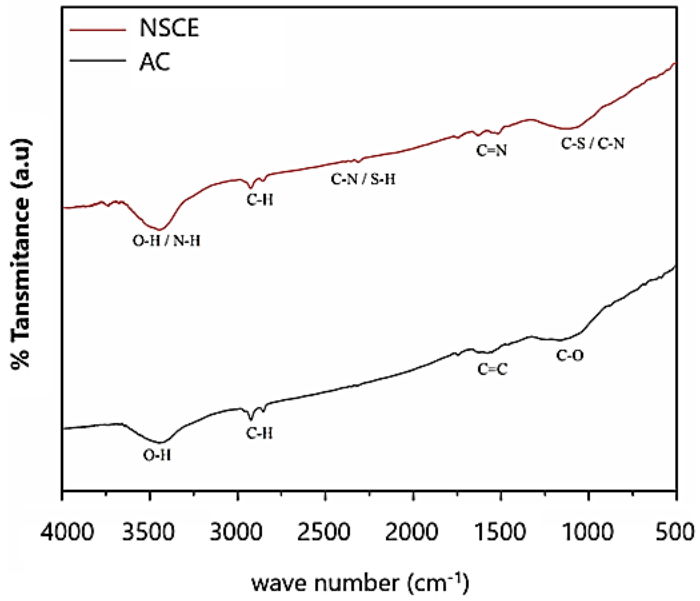

Figure 4. FTIR spectrum of the prepared-NSCE and the activated carbon (AC)

XPS analysis furthermore explains the presence of N and S within the carbon network. The XPS spectrum as shown by Fig. 5 shows C1s peak at 288.83 eV, 289.6 eV, 293.3 eV, and 304.86 eV, corresponding to C-C/ C=C, C-S, C-N, and C=O, respectively. The result is like N, P, and S doped-hard carbon prepared from the Camphor tree [7]. Sulfur (S_{2p}) can be observed at the binding energy of 168.26 eV and 169.55 eV, corresponding to $S_{2p3/2}$ and $S_{2p1/2}$ [7], and 171. 95 eV corresponds to C-SO_3-C [39], indicating the presence of S within the thiol group

DOI: 10.33961/jecst.2024.00017

attached to the carbon. A peak at 165 eV also confirms the presence of C-S and S-S bonds. The doped sulfur existed as thiophene sulfur (C4S). N1s reveal 402.4 eV and 405.5 eV, confirming pyrrolic nitrogen (N-5) and quaternary nitrogen (N-Q). N-5 can increase the diffusivity of Na^+, and N-Q can increase the conductivity of the carbon [31]. O1s revealed at 527.84 eV and 536.97 eV correspond to C=O and C-O [39]. Figure 6 describes the double N/S doped carbon's predicted structure and its surface morphology. The structure is drawn based on the XPS result and the doping reaction as indicated in equation (1).

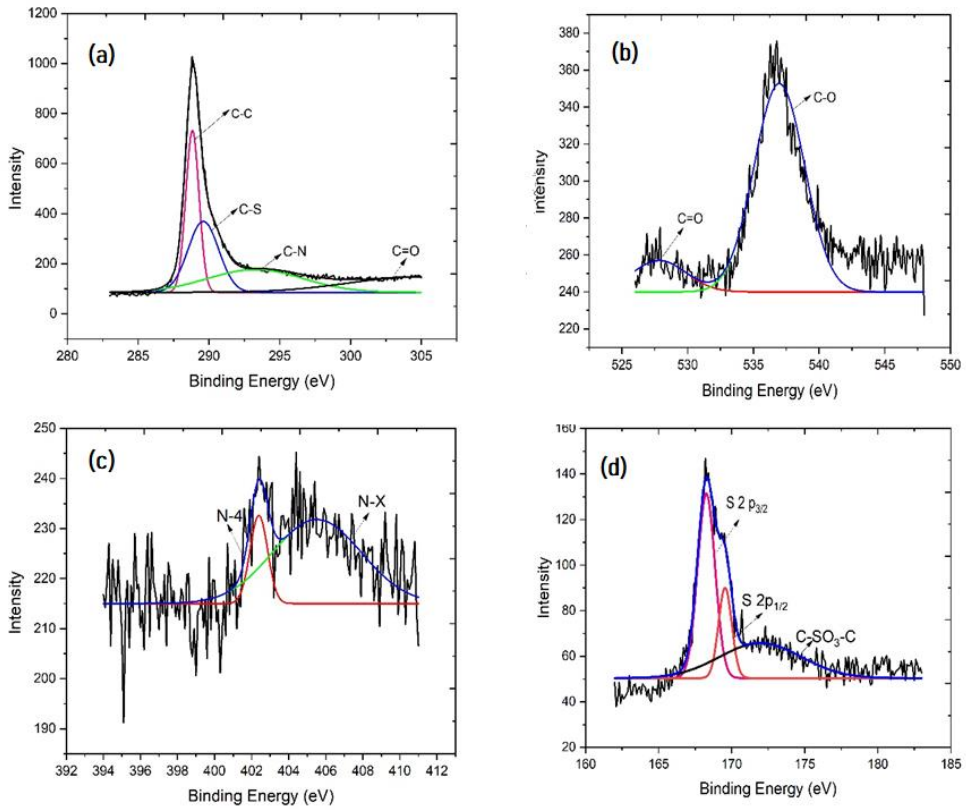

Figure 5. XPS analysis of the NSCE (a) C1s (b) O1s (c) N1s, and (d) S2p

DOI: 10.33961/jecst.2024.00017

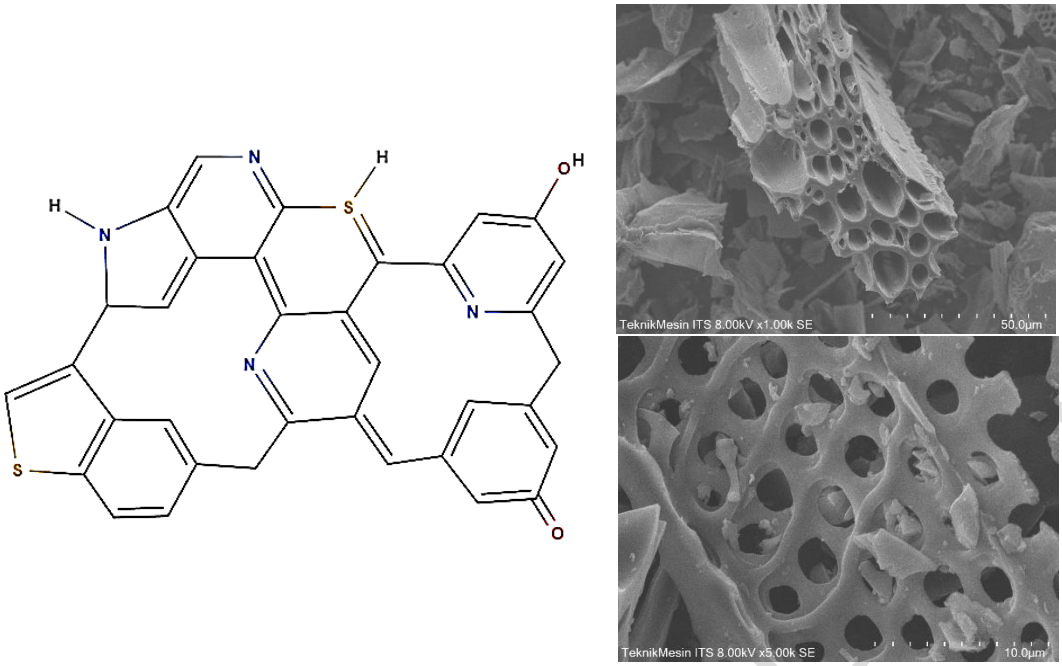

Figure 6. NSCE structure as predicted based on the XPS result and the doping reaction (eq. (1)), along with its surface morphology at different magnification

N/S doping to the activated carbon (ACB) has increased the specific conductivity from 2.42 x 10^{-1} S/cm to 23.74 x 10^{-1} S/cm at 20 Hz of frequency for the ACB and NSCE, respectively. Meanwhile, at a high frequency of 200 kHz, the conductivity increased from 3.06 x 10^{-1} S/cm for the ACB to 23.7 x 10^{-1} S/cm for the NSCE. The increasing is higher than a single N doping to the activated carbon, i.e., 5.41 x 10^{-1} S/cm, as found by our previous research [40].

CV analysis to NSCE | $NaClO_4$ | Na full cell is described in Figure 7, confirming quasi-reversible oxidation-reduction, attributed to solid-electrolyte Interface (SEI) formation [41,42], which lies between 0.764 V- 0.9 V. Figure 7 shows that the electrochemical reaction within the NSCE-$NaClO_4$-Na is reversible and consists of an onset potential at 0.1 V vs. Na/Na^+, representing Na oxidation and intercalation to the carbon network. The oxidation reached a maximum peak at 1.4 V vs. Na/Na^+ and then started to be reduced at an onset potential of 0.1 V vs. Na/Na+, then peaked at -0.98 V vs. Na/Na^+. Another research on carbon preparation from Camphor wood by HCl activation found that the oxidation peak started at 0.01 V and reached a peak at 0.15 V vs. Na/Na^+ at reduction started at

DOI: 10.33961/jecst.2024.00017

around 0.7 V vs. Na/Na^+ up to 0.01 V [43]. Previous research on biomass-derived carbon also found anodic-cathodic activity at 0 – 0.2 V vs. Na/Na+ as insertion and extraction of Na^+ in the carbon framework[44].

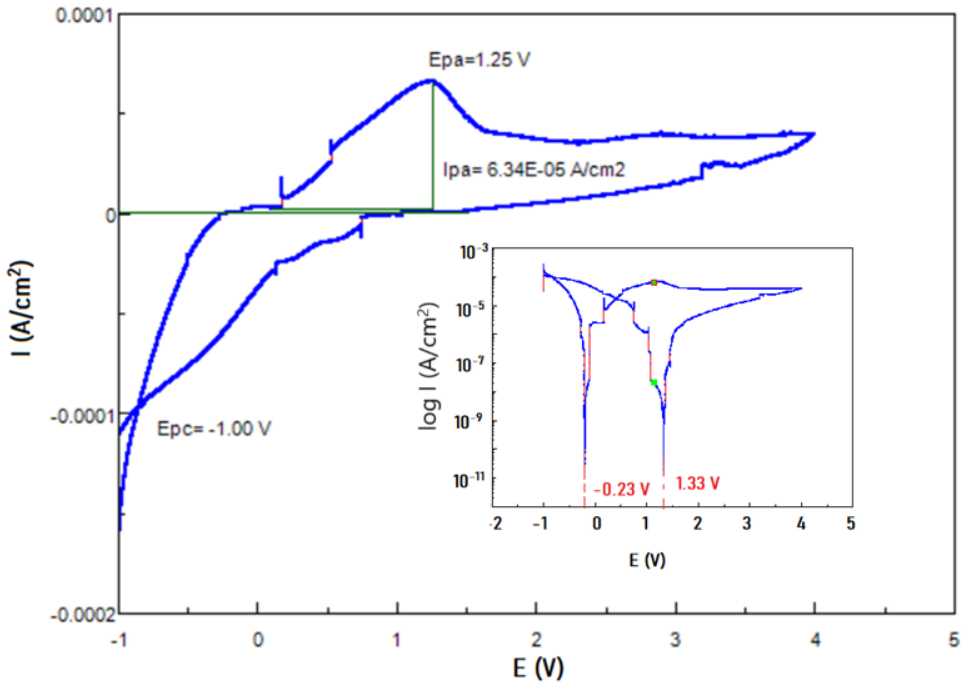

Figure 7. Cyclic Voltammogram of NSCE-$NaClO_4$-Na at -1 to 4 V vs Na/Na^+ at scan rate of 1 mV/s

The sodium battery NSCE-$NaClO_4$-Na shows an initial charging capacity of 720 mAh/g and an initial discharge capacity of 570 mAh/g at 0.2C, equal to 0.07 Ag^{-1} (1C= 372 mAh/g). The discharge capacity after the 4th cycle is 325 mAh/g, and the charging capacity remains constant at 385 mAh/g (Figure 8), resulting in a Coulombic efficiency of 84.4 %. The result is close to a sodium battery which was built from mango kernel derived-carbon with a discharge capacity of 328 mAh/g and Coulombic Efficiency of 86 % [45], and also close to a full sodium cell of NVP@C with biomass-hard carbon with 324.6 mAh/g of initial charge capacity [43]. This result is even higher than sodium full cell with $Na_{0.8}[Cu_{0.22}Fe_{0.30}Mn_{0.48}]O_2$ as cathode and seaweed derived-carbon as the anode, which produced ~180 mAh/g at 0.025 A/g of current rate [46]. The initial charging capacity is 400 mAh/g, and the discharge capacity

DOI: 10.33961/jecst.2024.00017

is 200 mAh/g at 0.5C (equal to 0.19 Ag^{-1}) current drawn. Meanwhile, the sodium battery with activated-bagasse carbon (ACB), the activated carbon before doped by N/S, shows an initial charging capacity of 270 mAh/g and the initial discharge capacity of 387 mAh/g at 0.07 Ag^{-1} (Figure 8.b), and at 0.19 Ag^{-1}, the charging capacity is 159 mAh/g and the discharge is 265 mAh/g and drop to 170 mAh/g after 4th cycle(Figure 8.d). It seems that 0.07 Ag-1 and 0.19 Ag^{-1} are high enough for the ACB sodium battery, and it caused an oscillation in voltage profile and prolong the discharge time. This happen because the voltages reached the upper limit (3 V) in a time longer than normal time[47]. Some comparisons are listed in Table 2.

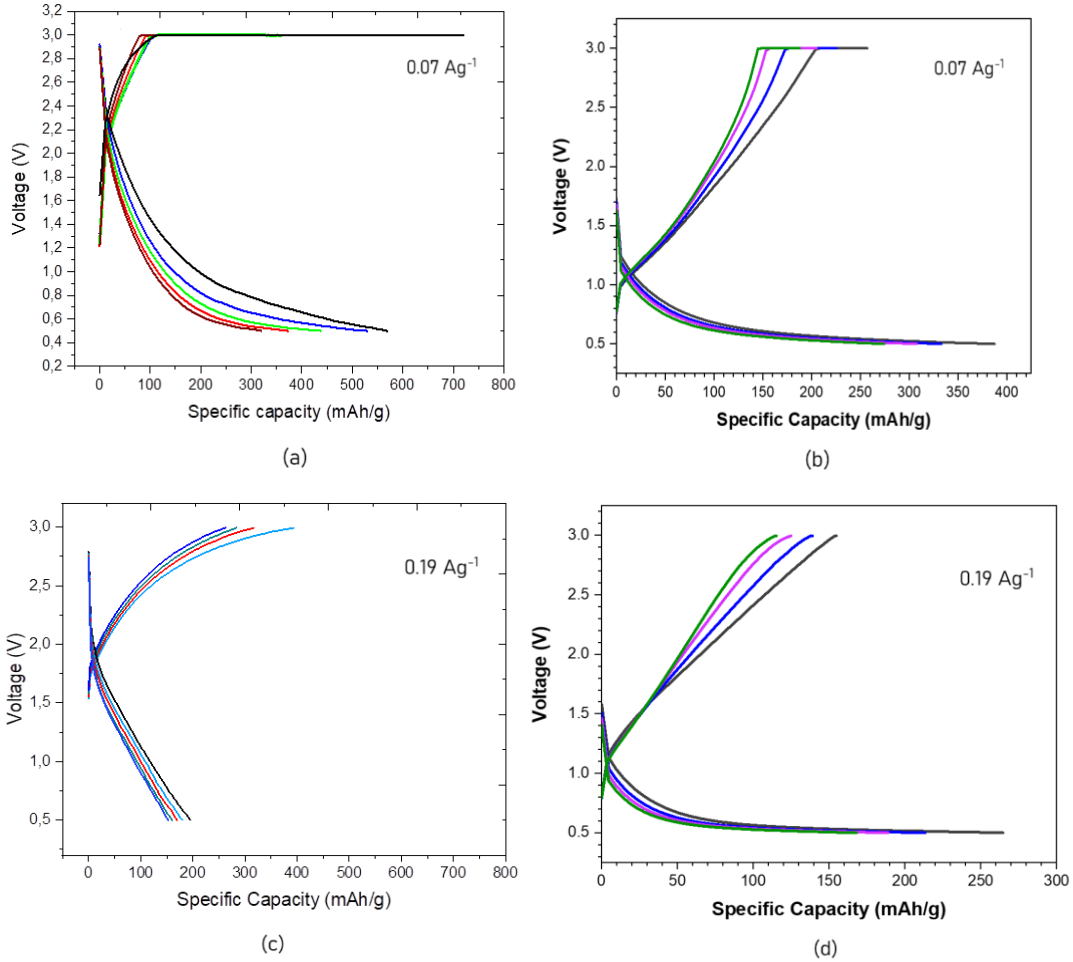

Figure 8. Charge-Discharge profile of the sodium NSCE battery (a,c), compared with the sodium ACB battery (b,d)

DOI: 10.33961/jecst.2024.00017

The cycle ability (Fig. 9) was done after the first 5 cycles of 0.5C current drawn. The battery shows a consistent capacity of ~200 mAh/g with a Coulombic efficiency of around 84.4 %, and capacity retention of around 57 % after 50 cycles. The result is even higher than a sodium full cell developed from mango kernel derived-carbon as anode and NVP ($Na_3V_2(PO_4)_3$) as cathode, which provides ~123 mAh/g and 113 mAh/g of charge and discharge capacity, respectively, at the end of 50 cycles [45].

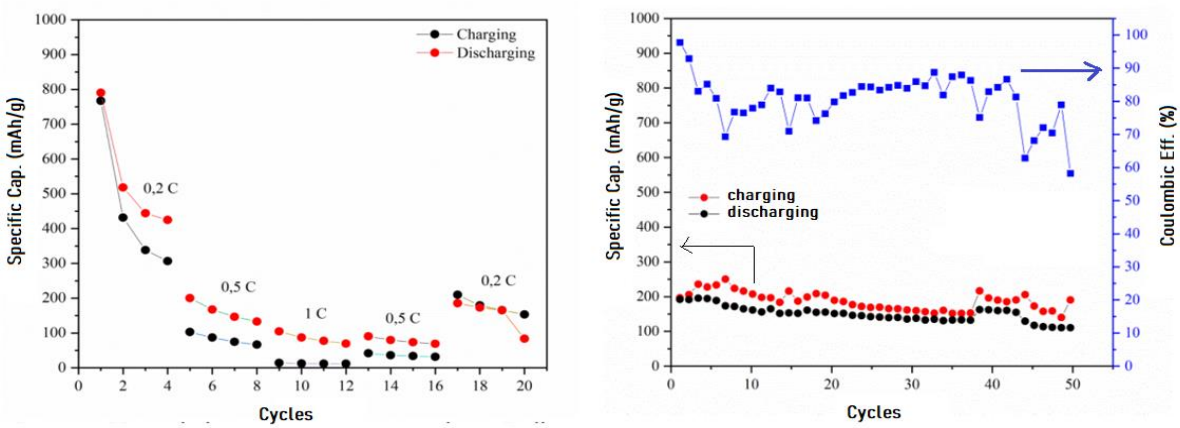

Figure 9. The cycling test performance the sodium NSCE battery at after 5th cycles of 0.19 Ag^{-1}

Impedance analysis after 50 cycles (Fig. 10) reveals two semi-circles as of 2800 Ω of ionic resistance and 2200 Ω of charge transfer electrode-electrolyte resistance. The resistance type is confirmed by 9.248 x 10^{-9} F and 1.44 x 10^{-7} F of ionic resistance and charge transfer resistance, respectively. The ionic resistance increases around 10 times after 50 cycles, indicating the formation of some resistive phases. Meanwhile, the charge transfer at electrode-electrolyte resistance rises to twice after 50 cycles, indicating the presence of an SEI layer between the electrode-electrolyte (separator).

DOI: 10.33961/jecst.2024.00017

Table 2. Some researches on biomass based- electrode for Sodium Ion Batteries

No.	Biomass	Materials	Charge capacity (mAh/g)/ current rate (Ag^{-1})	Discharge Capacity (mAh/g)/ current rate (Ag^{-1})	Coulombic Eff. (%)	Reference
1	Camphor tree	P/S-Cmph HCs N/S- Cmph HCs P/N/S- Cmph HCs	879.6 766.6 791.0		75.88 81.93 70.74	[48]
2	Olive seeds	Hard Carbon (HCs)		147.0	39.0	[49]
3	Mango Kernels	HCs	231.0	113.0/ 0.05	91.0	[45]
4	Chickpea husk	HCs		330.0/ 0.02		[50]
5	Camphor	HCs	324.6			[43]
6	Palm leaf	HCs		373.0/ 0.025		[51]
7	Lychee seeds	HCs	146.0/ 0.2 266.0 / 0.1			[52]
8	Rice husk	HCs	276.0			[53]
9	Spring Onion	S doped-C nanosheets	605.0 / 0.05 133.0 / 0.01			[39]
10	Seaweed	N doped-C	303.0/ 0.1 192.0/ 0.2			[46]
11	**Bagasse**	**N/S doped-C**	**720.0/ 0.07 400.0/ 0.19**	**570.0 / 0.07 200.0 / 0.19**	**84.4**	**This research**
12	Bagasse	Activated-C	260.0/ 0.07 259.0/ 0.19	383.0/ 0.07 262.0/ 0.19		This research

DOI: 10.33961/jecst.2024.00017

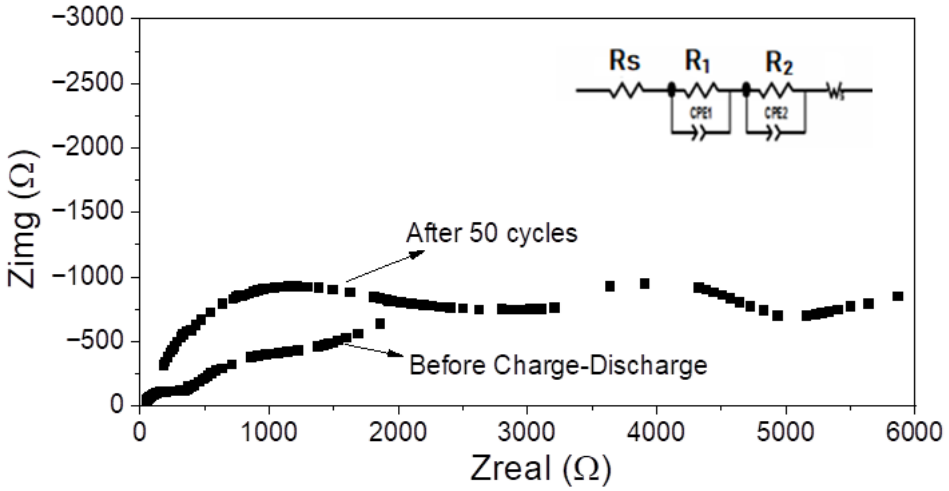

Figure 10. The impedance of the cycled-battery along with the R-C network model

CONCLUSION

The N/S doping to the prepared carbon from bagasse, a solid biomass produced by sugarcane production, initiates defect formation in the carbon network, as proven by the increasing Raman I_D/I_G ratio. The doped sulfur existed as thiophene sulfur (C4S). Meanwhile, N1s reveal 402.4 eV and 405.5 eV, confirming pyrrolic nitrogen (N-5) and quaternary nitrogen (N-Q). N-5 can increase the diffusivity of Na^+, and N-Q can increase the conductivity of the carbon. The produced-N/S doped carbon (NSCE) is a suitable electrode for sodium-ion batteries by delivering the initial charge-discharge capacity of 720 mAh/g and 570 mAh/g, respectively, at 0.2 C (0.07 Ag^{-1}). The battery has a capacity retention of 57 % after 50 cycles, a stable 200 mAh/g capacity, and a Coulombic efficiency of 84.4 %.

ACKNOWLEDGEMENT

The authors acknowledge Sebelas Maret University for funding this research through an International Collaborative Research with a contract number of 228/UN27.22/PT.01.03/2023. A part of this work was conducted in The University of Electro-Communications Coordinated Centre for UEC Research Facilities, supported by Advanced Research Infrastructure for

DOI: 10.33961/jecst.2024.00017

Materials and Nanotechnology in Japan (ARIM) of the Ministry of Education, Culture, Sports, Science and Technology (MEXT). The authors also acknowledge Mr. Yajima's assistance with the XPS analysis.

Declaration. On behalf of all authors, the corresponding author states that there is no conflict of interest.

REFERENCE

[1] Li X, Zeng X, Ren T, Zhao J, Zhu Z, Sun S, et al. The transport properties of sodium-ion in the low potential platform region of oatmeal-derived hard carbon for sodium-ion batteries. J Alloys Compd 2019;787:229–38. https://doi.org/10.1016/j.jallcom.2019.02.077.

[2] Slater MD, Kim D, Lee E, Johnson CS. Sodium-Ion Batteries. Adv Funct Mater Mater 2013;23:947–58. https://doi.org/10.1002/adfm.201200691.

[3] Larcher D, Tarascon J-M. Towards greener and more sustainable batteries for electrical energy storage. Nat Chem 2015;7:19–29. https://doi.org/10.1038/nchem.2085.

[4] Wang L, Zhao X, Dai S, Shen Y, Wang M. High-rate and stable iron phosphide nanorods anode for sodium-ion battery. Electrochim Acta 2019;314:142–50. https://doi.org/10.1016/j.electacta.2019.05.071.

[5] Xiang J, Lv W, Mu C, Zhao J, Wang B. Activated hard carbon from orange peel for lithium/sodium ion battery anode with long cycle life. J Alloys Compd 2017;701:870–4. https://doi.org/10.1016/j.jallcom.2017.01.206.

[6] Alvin S, Yoon D, Chandra C, Cahyadi HS, Park JH, Chang W, et al. Revealing sodium ion storage mechanism in hard carbon. Carbon N Y 2019;145:67–81. https://doi.org/10.1016/j.carbon.2018.12.112.

[7] Aristote NT, Song Z, Deng W, Hou H, Zou G, Ji X. Effect of double and triple-doping of sulfur, nitrogen and phosphorus on the initial coulombic efficiency and rate performance of the biomass derived hard carbon as anode for sodium-ion batteries. J Power Sources 2023;558:232517. https://doi.org/10.1016/j.jpowsour.2022.232517.

[8] Meng Y, Lin R, Duan M, Du M, Zhang H, Ren G, et al. Heteroatom-doped nanoporous carbon with high rate performance as anode for sodium-ion batteries. J Mater Sci Sci Mater Electron 2021;32:8295–8303. https://doi.org/https://link.springer.com/article/10.1007/s10854-021-05343-5.

[9] Jin Q, Li W, Wang K, Li H, Feng P, Zhang Z, et al. Tailoring 2D Heteroatom-Doped Carbon Nanosheets with Dominated Pseudocapacitive Behaviors Enabling Fast and High-Performance Sodium Storage. Adv Funct Mater 2020;30:1909907. https://doi.org/10.1002/adfm.201909907.

[10] Shen F, Luo W, Dai J, Yao Y, Zhu M, Hitz E, et al. Ultra-Thick, Low-Tortuosity, and

DOI: 10.33961/jecst.2024.00017

Mesoporous Wood Carbon Anode for High-Performance Sodium-Ion Batteries. Adv Energy Mater 2016;6:1600377. https://doi.org/10.1002/aenm.201600377.

[11] Lotfabad EM, Ding J, Cui K, Kohandehghan A, Kalisvaart WP, Hazelton M, et al. High-Density Sodium and Lithium Ion Battery Anodes from Banana Peels. ACS Nano 2014;8:7115–29. https://doi.org/10.1021/nn502045y.

[12] Li Y, Hu Y-S, Titirici M-M, Chen L, Huang X. Hard Carbon Microtubes Made from Renewable Cotton as High-Performance Anode Material for Sodium-Ion Batteries. Adv Energy Mater 2016;6:1600659. https://doi.org/10.1002/aenm.201600659.

[13] Qin D, Liu Z, Zhao Y, Xu G, Zhang F, Zhang X. A sustainable route from corn stalks to N, P-dual doping carbon sheets toward high performance sodium-ion batteries anode. Carbon N Y 2018;130:664–71. https://doi.org/10.1016/j.carbon.2018.01.007.

[14] Simone V, Boulineau A, de Geyer A, Rouchon D, Simonin L, Martinet S. Hard carbon derived from cellulose as anode for sodium ion batteries: Dependence of electrochemical properties on structure. J Energy Chem 2016;25:761–8. https://doi.org/10.1016/j.jechem.2016.04.016.

[15] Qiu S, Xiao L, Sushko ML, Han KS, Shao Y, Yan M, et al. Manipulating Adsorption–Insertion Mechanisms in Nanostructured Carbon Materials for High-Efficiency Sodium Ion Storage. Adv Energy Mater 2017;7:1700403. https://doi.org/10.1002/aenm.201700403.

[16] Wang Q, Zhu X, Liu Y, Fang Y, Zhou X, Bao J. Rice husk-derived hard carbons as high-performance anode materials for sodium-ion batteries. Carbon N Y 2018;127:658–66. https://doi.org/10.1016/j.carbon.2017.11.054.

[17] Liu Y, Lee DJ, Lee Y, Raghavan P, Yang R, Ramawati F, et al. Biomass-Derived Three-Dimensionally Connected Hierarchical Porous Carbon Framework for Long-Life Lithium – Sulfur Batteries 2022;28:97–102.

[18] Dwiyaniti M, Elang Barruna AG, Muhamad Naufal R, Subiyanto I, Setiabudy R, Hudaya C. Extremely high surface area of activated carbon originated from sugarcane bagasse. IOP Conf Ser Mater Sci Eng 2020;909. https://doi.org/10.1088/1757-899X/909/1/012018.

[19] Heniegal AM, Ramadan MA, Naguib A, Agwa IS. Study on properties of clay brick incorporating sludge of water treatment plant and agriculture waste. Case Stud Constr Mater 2020;13:e00397. https://doi.org/10.1016/j.cscm.2020.e00397.

[20] Rahmawati LA. Studi Literatur Produksi Bioethanol dari Ampas Tebu dengan Metode Pyrolisis. J Enviscience 2020;4:46. https://doi.org/10.30736/4ijev.v4iss1.131.

[21] Rahmawati F, Ridassepri AF, Chairunnisa, Wijayanta AT, Nakabayashi K, Miyawaki J, et al. Carbon from bagasse activated with water vapor and its adsorption performance for methylene blue. Appl Sci 2021;11:1–16. https://doi.org/10.3390/app11020678.

[22] Chairunnisa, K. Thu, T. Miyazaki, Nakabayashi K, Miyawaki J, A. T. Wij ayanta, et al. Highly Microporous Activated Carbon from Acorn Nutshells and its Performance in Water Vapor Adsorption. Evergreen 2021;8:249–54. https://doi.org/10.5109/4372285.

[23] Ridassepri AF, Rahmawati F, Heliani KR, Chairunnisa, Miyawaki J, Wijayanta AT.

DOI: 10.33961/jecst.2024.00017

Activated carbon from bagasse and its application for water vapor adsorption. Evergreen 2020;7:409–16. https://doi.org/10.5109/4068621.

[24] Tao H, Zhang H, Li J, Ding W. Biomass based activated carbon obtained from sludge and sugarcane bagasse for removing lead ion from wastewater. Bioresour Technol 2015;192:611–7. https://doi.org/10.1016/j.biortech.2015.06.006.

[25] Luo X, Cai Y, Zeng J. Cr (VI) adsorption performance and mechanism of an effective activated carbon prepared from bagasse with a one-step pyrolysis and ZnCl 2 activation method. Cellulose 2019;26:4921–34. https://doi.org/10.1007/s10570-019-02418-9.

[26] Solís-Fuentes JA, Galán-Méndez F, Hernández-Medel M del R, García-Gómez RS, Bernal-González M, Mendoza-Pérez S, et al. Effectiveness of bagasse activated carbon in raw cane juice clarification. Food Biosci 2019;32:100437. https://doi.org/10.1016/j.fbio.2019.100437.

[27] Gao S, Chen Y, Su J, Wang M, Wei X, Jiang T, et al. Triboelectric Nanogenerator Powered Electrochemical Degradation of Organic Pollutant Using Pt-Free Carbon Materials. ACS Nano 2017;11:3965–72. https://doi.org/10.1021/acsnano.7b00422.

[28] Xiong P, Zhao X, Xu Y. Nitrogen-Doped Carbon Nanotubes Derived from Metal-Organic Frameworks for Potassium-Ion Battery Anodes. ChemSusChem 2018;11:202–8. https://doi.org/10.1002/cssc.201701759.

[29] Wan H, Hu X. Nitrogen/sulfur co-doped disordered porous biocarbon as high performance anode materials of lithium/sodium ion batteries. Int J Hydrogen Energy 2019;44:22250–62. https://doi.org/10.1016/j.ijhydene.2019.06.107.

[30] Ingemarsson L, Halvarsson M. EDX/SEM Analysis of Boron. Chalmers Univerisity Technol 2011:1–15.

[31] Guo F, Jiang X, Jia X, Liang S, Qian L, Rao Z. Synthesis of biomass carbon electrode materials by bimetallic activation for the application in supercapacitors. J Electroanal Chem 2019;844:105–15. https://doi.org/10.1016/j.jelechem.2019.05.004.

[32] Sun S, Yu Q, Li M, Zhao H, Wu C. Preparation of coffee-shell activated carbon and its application for water vapor adsorption. Renew Energy 2019;142:11–9. https://doi.org/10.1016/j.renene.2019.04.097.

[33] Puziy A., Poddubnaya O., Martínez-Alonso A, Suárez-García F, Tascón JM. Synthetic carbons activated with phosphoric acid. Carbon N Y 2002;40:1493–505. https://doi.org/10.1016/S0008-6223(01)00317-7.

[34] Zhang L, Tu LY, Liang Y, Chen Q, Li ZS, Li CH, et al. Coconut-based activated carbon fibers for efficient adsorption of various organic dyes. RSC Adv 2018;8:42280–91. https://doi.org/10.1039/c8ra08990f.

[35] Ahmed Baloch H, Nizamuddin S, Siddiqui MTH, Mubarak NM, Dumbre DK, Srinivasan MP, et al. Sub-supercritical liquefaction of sugarcane bagasse for production of bio-oil and char: Effect of two solvents. J Environ Chem Eng 2018;6:6589–601. https://doi.org/10.1016/j.jece.2018.10.017.

[36] Li D, Zhang L, Chen H, Ding L-X, Wang S, Wang H. Nitrogen-doped bamboo-like carbon nanotubes: promising anode materials for sodium-ion batteries. Chem Commun 2015;51:16045–8. https://doi.org/10.1039/C5CC06266G.

DOI: 10.33961/jecst.2024.00017

[37] Zhang Y, Sun Z, Wang H, Wang Y, Liang M, Xue S. Nitrogen-doped graphene as a cathode material for dye-sensitized solar cells: Effects of hydrothermal reaction and annealing on electrocatalytic performance. RSC Adv 2015;5:10430–9. https://doi.org/10.1039/c4ra13224f.

[38] Luo X, Zhang W, Han Y, Chen X, Zhu L, Tang W, et al. N,S co-doped carbon dots based fluorescent "on-off-on" sensor for determination of ascorbic acid in common fruits. Food Chem 2018;258:214–21. https://doi.org/10.1016/j.foodchem.2018.03.032.

[39] Zhao G, Yu D, Zhang H, Sun F, Li J, Zhu L, et al. Sulphur-doped carbon nanosheets derived from biomass as high-performance anode materials for sodium-ion batteries. Nano Energy 2020;67:104219. https://doi.org/10.1016/j.nanoen.2019.104219.

[40] Rahmawati F, Ridassepri AF, Heraldy E, Wijayanta AT, Rohendi D, Purwaningsih D. Single N- and double N/S- doping into steam activated- carbon from solid waste of sugarcane production as a potential material for electrode. Acta Polytech 2024;under revi.

[41] Bai P, Han X, He Y, Xiong P, Zhao Y, Sun J, et al. Solid electrolyte interphase manipulation towards highly stable hard carbon anodes for sodium ion batteries. Energy Storage Mater 2020;25:324–33. https://doi.org/10.1016/j.ensm.2019.10.006.

[42] Pan J, Sun Y, Yan Y, Feng L, Zhang Y, Lin A, et al. Revisit Electrolyte Chemistry of Hard Carbon in Ether for Na Storage. JACS Au 2021;1:1208–16. https://doi.org/10.1021/jacsau.1c00158.

[43] Guo S, Chen Y, Tong L, Cao Y, Jiao H, long Z, et al. Biomass hard carbon of high initial coulombic efficiency for sodium-ion batteries: Preparation and application. Electrochim Acta 2022;410:140017. https://doi.org/10.1016/j.electacta.2022.140017.

[44] Kumaresan TK, Masilamani SA, Raman K, Karazhanov SZ, Subashchandrabose R. High performance sodium-ion battery anode using biomass derived hard carbon with engineered defective sites. Electrochim Acta 2021;368:137574. https://doi.org/10.1016/j.electacta.2020.137574.

[45] Bhawana K, Roy A, Chakrabarty N, Gautam M, Dutta DP, Mitra S. Sodium-ion batteries: Chemistry of biomass derived disordered carbon in carbonate and ether-based electrolytes. Electrochim Acta 2022;425:140744. https://doi.org/10.1016/j.electacta.2022.140744.

[46] Senthil C, Park JW, Shaji N, Sim GS, Lee CW. Biomass seaweed-derived nitrogen self-doped porous carbon anodes for sodium-ion batteries: Insights into the structure and electrochemical activity. J Energy Chem 2021;64:286–95. https://doi.org/10.1016/j.jechem.2021.04.060.

[47] Zarei-Jelyani M. Re: if discharge capacity is higher than charge capacity in lithium ion half cell from anode?. 2018. https://www.researchgate.net/post/if_discharge_capacity_is_higher_than_charge_capacity_in_lithium_ion_half_cell_from_anode/5acdbab0f7b67eeccb3cc99a/citation/download.

[48] Aristote NT, Zou K, Di A, Deng W, Wang B, Deng X, et al. Methods of improving the initial Coulombic efficiency and rate performance of both anode and cathode materials for sodium-ion batteries. Carbon Lett 2022;33:730–42.

DOI: 10.33961/jecst.2024.00017

[49] Bensouda H, Hakim C, Aziam H, Bacaoui A, Saadoune I. Effect of NaOH impregnation on the electrochemical performances of hard carbon derived from olive seeds biomass for sodium ion batteries. Mater Today Proc 2021;51:2066–70. https://doi.org/10.1016/j.matpr.2022.01.337.

[50] Ghani U, Iqbal N, Aboalhassan AA, Liu B, Aftab T, Zada I, et al. One-step sonochemical fabrication of biomass-derived porous hard carbons; towards tuned-surface anodes of sodium-ion batteries. J Colloid Interface Sci 2022;611:578–87. https://doi.org/10.1016/j.jcis.2021.12.104.

[51] Nie W, Cheng H, Liu X, Sun Q, Tian F, Yao W, et al. Surface organic nitrogen-doping disordered biomass carbon materials with superior cycle stability in the sodium-ion batteries. J Power Sources 2022;522:230994. https://doi.org/10.1016/j.jpowsour.2022.230994.

[52] Raj K A, Panda MR, Dutta DP, Mitra S. Bio-derived mesoporous disordered carbon: An excellent anode in sodium-ion battery and full-cell lab prototype. Carbon N Y 2019;143:402–12. https://doi.org/10.1016/j.carbon.2018.11.038.

[53] Rybarczyk MK, Li Y, Qiao M, Hu YS, Titirici MM, Lieder M. Hard carbon derived from rice husk as low cost negative electrodes in Na-ion batteries. J Energy Chem 2019;29:17–22. https://doi.org/10.1016/j.jechem.2018.01.025.

DOI: 10.33961/jecst.2024.00017